UC Berkeley College of Chemistry

Chemistry 125

Physical Chemistry Laboratory

Pulse NMR Spectroscopy

Author:

Jonathan Melville

Collaborators:

Donghwa Kim and David Gygi

Graduate Student Instructor:

Jon Raberg

December 8, 2014

1 Abstract

Using pulsed nuclear magnetic resonance (NMR), spin-lattice and spin-spin relaxation times (T_1 and T_2, respectively) were measured for mineral oil and various concentrations of aqueous copper (II) sulfate. Both T_1 and T_2 exhibit a strong diffusion dependence (reflective of the viscosity of the solvent), as well as an exponential decay relative to the concentration of paramagnetic copper (II) ions in solution. Spin-lattice relaxation times were measured using an inversion-recovery sequence, whereas spin-spin relaxation times were calculated using Meiboom-Gill spin-echo sequences (and, for reference, more prototypical Hahn spin-echo sequences). Potential sources for error include inhomogeneities in the magnetic field, the presence of dissolved paramagnetic O_2, and temperature variation over the course of the experiment.

2 Introduction

An understanding of the spin relaxation times of a system is useful for a variety of reasons across multiple fields, often due to the ability to image samples by comparing the relaxation rate of component. This process is often known, aptly, as magnetic resonance imaging (MRI), and is often used to generate cross-sectional images of biological samples by comparing the T_1 and T_2 relaxation times of water across various tissue types. Cancerous tumors can be identified by their different T_1 and T_2 relaxation times from the surrounding tissue – for example, breast tissue normally has a T_1 relaxation time of 367 ± 79 ms, but a breast tumor will have T_1 relaxation times of 1080 ± 80 ms[1]. Obviously, the ability to actively detect cancerous masses without physical surgery has tremendous benefits for oncologists and their patients.

This imaging is achieved by exposing the sample to a magnetic field, generating a net nuclear magnetization. Then, an electromagnetic pulse of the correct length at the corresponding resonant frequency can rotate the magnetization vector by a specified angle, and the relaxation rate of the magnetization to its equilibrium value can be calculated; the relaxation times T_1 and T_2 are time constants for this decay[10].

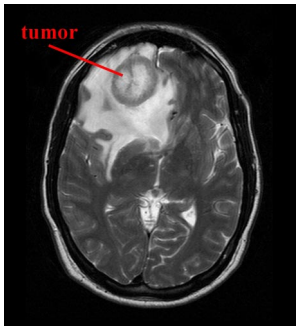

Figure 1: An MRI image, showing a brain tumor resolved from surrounding brain tissue by its different T_1 relaxation time.

Nuclear magnetic resonance fundamentally depends upon the nuclear spin (I) of an atom, which is a function of the number of protons and neutrons in its nucleus. Some atoms, such as $^{12}C_6$ or $^{32}S_{16}$, have no intrinsic nuclear spin, though that does not mean that isotopes of these elements cannot have nuclear spin ($^{13}C_6$ and $^{33}S_{16}$). In this experiment, we concern ourselves with hydrogen, which has a nuclear spin $I = \frac{1}{2}$. Any nucleus with a nuclear spin $I \geq \frac{1}{2}$ has a magnetic dipole moment μ oriented in the same direction as the nuclear spin I, that can be calculated using Equation 1:

$$\mu = \gamma \hbar I, \tag{1}$$

where γ is the gyromagnetic ratio of the nucleus in question ($2.675 \times 10^8 \frac{\text{rad}}{\text{T}\cdot\text{s}}$ for hydrogen). When an external magnetic field of strength B_0 is applied to a system like this, it induces a splitting of states due to the Zeeman effect; in the case of hydrogen, there are only two possible states ($m = \pm\frac{1}{2}$), with an energy splitting of

$$\Delta E = \gamma \hbar B_0. \tag{2}$$

In the absence of an external magnetic field, the two states $m = \pm\frac{1}{2}$ are of equal energy and are thus equally populated; however, when a magnetic field is applied, the energies are changed and the states become unequally populated, bringing about a net equilibrium magnetization M_0 in the direction of the magnetic field. If the system, having come to equilibrium in the magnetic field, is then excited by an electromagnetic pulse with energy matching the splitting ΔE, spins will be excited from the lower to the higher

energy state. This process induces a change in the net magnetization of the system, which will gradually return to its equilibrium value through a variety of relaxation processes[10].

In this experiment, we primarily concern ourselves with spin-lattice (T_1) and spin-spin (T_2) relaxation times. Spin-lattice relaxation time (so called because energy gained from the electromagnetic pulse must be dissipated through the lattice of the matrix) is defined in terms of the relaxation of the z-component of magnetization (M_z) after it has been inverted by a 180° "π-pulse", and is characterized by Equation 3:

$$M_z(t) = M_0 \left[1 - \exp\left(-\frac{t}{T_1}\right)\right], \tag{3}$$

where T_1 is the time constant of the exponential decay, or the time it takes for the net magnetization to decay to e^{-1} ($\approx 36.8\%$) of its original value. However, the presence of the large external magnetic field B_0 occludes the measurement of magnetization in the z-direction (the assumed direction of B_0). To circumvent this, the inverted magnetization can be subjected to a rotating $\pi/2$-pulse a time t after the inverting π-pulse, which shifts the magnetization vector into the xy-plane, where it can be measured without being drowned out by the large external magnetic field. Performing this operation, known as an inversion-recovery sequence, for various times t can allow for the time constant T_1 to be determined using Equation 3.

While spin-lattice relaxation time concerns itself with the relaxation of an inverted magnetization, spin-spin relaxation is the process by which spins rotated into the xy-plane by a $\pi/2$-pulse decay back to the z-axis. This process is known as spin-spin relaxation because the nuclei relax to their equilibrium magnetization in the z-direction through interactions with each other, not the matrix. Brownian motion of atomic nuclei, coupled with the intrinsic spin of each nucleus, generates localized oscillating magnetic fields that can occasionally stimulate spin relaxation in nearby nuclei by resonating with the Larmor precession frequency. This phenomenon is characterized by Equation 4:

$$M_{xy}(t) = M_0 \exp\left(-\frac{t}{T_2}\right), \tag{4}$$

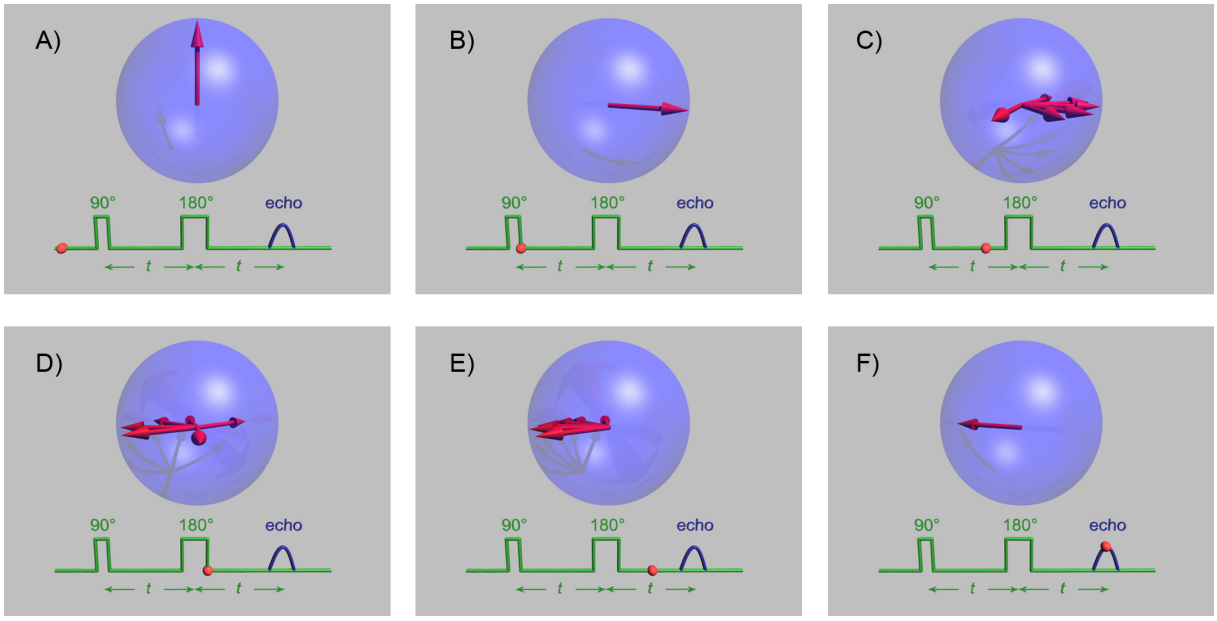

Figure 2: A graphic depicting the steps of the Hahn spin-echo sequence[7].

where T_2 is the time constant of the exponential decay, equal to the time it takes for the magnetization in the xy-plane to decay to e^{-1} ($\approx 36.8\%$) of its equilibrium value. However, a direct measurement of the decay of the magnetization is nontrivial, because inhomogeneities of the external magnetic field cause the sample spins to decohere in the xy-plane before total relaxation to the z-axis. The Hahn spin-echo sequence (and later the Carr-Purcell and Meiboom-Gill sequences) overcame this by using an inverting π-pulse some time τ after the spins are rotated into the xy-plane, pictured in Figure 2. The π-pulse inverts the spins, but does not alter their momenta, so the decoherence process reverses itself and after another time period τ a coherent signal – the echo – can be measured. By varying the time τ and measuring the signals at coherence (2τ), a fit for Equation 4 can be achieved and T_2 can be calculated[6].

However, an inconsistency in the basic Hahn spin-echo sequence, as described, becomes evident; the decoherence and subsequent recoherence of the spins is proportional to the magnitude of the Larmor precession, which is a function of the external magnetic field B_0. Since the external field is not perfectly homogeneous, as each nucleus undergoes a random walk through the solution it will experience different magnetic fields, meaning that the dephasing speed is not time-invariant as the Hahn spin-echo sequence assumes. Moreover, since this defect corresponds with the diffusion of particles throughout the

sample, the magnitude of this defect will vary inversely with the viscosity of the solvent.

Carr and Purcell improved upon Hahn's work by applying multiple periodic π-pulses to the sample, producing a sequence of decaying echoes that maintain the dephasing speed determined by the Larmor precession during the initial π/2-pulse. This process essentially allows for multiple Hahn spin-echo measurements to be taken at once, while reducing the errors caused by inhomogeneities in the magnetic field. However, the Carr-Purcell sequence suffers from the compounding of errors in the π-pulses, which can falsely reduce apparent measured relaxation times; if the π-pulses are off even the slightest amount from a perfect 180° pulse, a small fraction of the magnetization vector from the xy-plane will be shunted into the z-axis and will not be measured. Each subsequent inversion will suffer the same loss of signal, causing the entire sequence to fall artificially short[2].

Meiboom and Gill further improved upon the process by introducing a π/2 dephasing in the original π/2-pulse, causing subsequent π-pulses to invert the vector in the opposite direction, such that each pulse in a series essentially error-corrects for any deviation in the previous pulse. With this method, an accurate calculation of spin-spin relaxation times can be achieved[8].

In this experiment, T_1 was calculated using an inversion-recovery sequence, and T_2 was calculated using both a Meiboom-Gill sequence (for accuracy) and a Hahn spin-echo sequence (to show the diffusion dependence of the relaxation time).

3 Experimental

3.1 Instrumental

In this experiment, a Hewlett-Packard 54630B Oscilloscope with 0.35 T Helmholtz electromagnet was used to analyze presealed samples. Reagents were acquired from your friendly neighborhood chem stockroom.

3.2 Procedure

Each sample, contained within a presealed glass tube with stopper, had an O-ring placed around it to ensure field consistency across samples, to minimize inhomogeneities in the magnetic field that would cause peak broadening. To maximize signal-to-noise ratio, a resonant frequency was determined that maximized signal, by varying the frequency around the known value of 15.00000 MHz, and the detector signal was checked to ensure it matched the mixer signal. Next, pulses were programmed on two separate channels to generate the desired sequence – inversion-recovery, Hahn spin-echo, or Meiboom-Gill. A repetition time was set to ensure that pulses did not overlap, and the instrument was set to bin consecutive scans to reduce fluctuations and allow for measurements to be read off more easily. For each sequence, 20 data points were generated and noted down; instrumental parameters are summarized in Table 1.

Sample	**Sequence**	**Freq. (MHz)**	**Rep. Time (ms)**	**# Pulses**
Mineral Oil	Inversion-Recovery	14.98730	100	1
	Hahn Spin-Echo	14.98730	100	1
	Meiboom-Gill	14.98730	100	20
$CuSO_4$ (10 mM)	Inversion-Recovery	14.98300	1000	1
	Hahn Spin-Echo	14.98300	100	1
	Meiboom-Gill	14.98300	100	20
$CuSO_4$ (50 mM)	Inversion-Recovery	14.98300	1000	1
	Hahn Spin-Echo	14.98300	100	1
	Meiboom-Gill	14.98300	100	20
$CuSO_4$ (100 mM)	Inversion-Recovery	14.98300	1000	1
	Hahn Spin-Echo	14.98300	100	1
	Meiboom-Gill	14.98300	100	20

Table 1: Instrumental parameters for all samples.

For each sample, an inversion-recovery sequence was programmed first, with a π-pulse followed by a $\pi/2$-pulse. In this experiment, the net magnetization relaxes from an initial excited state of $-B_0$ to $+B_0$; however, the instrument only provides positive values, so the apparent value dropped rapidly to 0 and then slowly rose, asymptotically approaching its initial value. Next, a Hahn spin-echo sequence was set, with a $\pi/2$-pulse followed by a π-pulse. Measurements were taken down for various time-delays. Finally, for the Meiboom-Gill sequence, a $\pi/2$-pulse followed by 20 π-pulses was set, with a set delay time

τ, such that the time of the nth echo peak relative to the initial π/2-pulse would be

$$t = (2n + 1)\tau. \tag{5}$$

4 Results

4.1 Data Analysis

Since the relative populations of the equilibrium excited and ground states follow a Boltzmann distribution, they can be easily calculated to determine the relative population of states in the system. Using Equations 1 and 2 on page 2, and knowing that the energy of a photon follows trivially from its frequency (Equation 6), we can find the frequency of light that can overcome a field of strength B_0 (or, conversely, the magnetic field that can be overcome by light of frequency ν).

$$E = h\nu \tag{6}$$

$$B_0 = \frac{2\pi\nu}{\gamma} \tag{7}$$

Plugging this derived value for B_0 into a simple Boltzmann distribution (Equation 8), we can derive a term for the relative population $\frac{N_{\text{opposed}}}{N_{\text{aligned}}}$:

$$\frac{N_{\text{opposed}}}{N_{\text{aligned}}} = e^{\frac{-\gamma\hbar B_0}{k_B T}} \tag{8}$$

$$1 - \frac{N_{\text{opposed}}}{N_{\text{aligned}}} = \frac{N_{\text{aligned}} - N_{\text{opposed}}}{N_{\text{aligned}}} = \frac{4\pi\hbar I\nu}{k_B T}. \tag{9}$$

Plugging values into this equation, we can determine that the relative population $\frac{N_{\text{opposed}}}{N_{\text{aligned}}} \approx 0.999$, showing that the splitting in this weak magnetic field is easily broached by even room-temperature thermal fluctuations.

To determine the spin-lattice and spin-spin relaxation times, Equations 3 and 4 on

page 3 must be rearranged into a form that facilitates regression from the acquired data. This can be done by rearranging the equations as first-order functions of the delay time τ (or, in the case of the Meiboom-Gill sequence, the cumulative time t after a series of pulses, calculated from the delay time between pulses and then number of pulses), where the slope of the resulting line is related to the time constant of relaxation. Alternatively, a cruder method can be used in which the exponential decay is plotted and the time constant is estimated as the time at which the net magnetization decays to $e^{-1} \approx 36.8\%$ of its initial value; however, the linear regression method is more mathematically robust and allows for more rigorous data and error analysis using least-squares fitting.

$$\ln\left(\frac{M_0 - M(\tau)}{M_0}\right) = -\frac{1}{T_1}\tau \tag{10}$$

Equation 10 allows for the calculation of T_1 from the inversion-recovery sequence, where the slope of the linear regression is the negative reciprocal of the time constant T_1.

$$\ln\left(M(\tau)\right) = -\frac{1}{T_2}t + \ln\left(M_0\right); t = 2(n+1)\tau \tag{11}$$

Equation 11 calculates T_2 from the Meiboom-Gill series, where the slope of the linear regression is the negative reciprocal of the time constant T_2. Since the Meiboom-Gill series consists of many pulses separated by a time constant τ, the cumulative time t for this sequence must be separately calculated as a function of the pulse number and the time delay, as seen in Equation 5 on page 7.

$$\ln\left(M(\tau)\right) = -\frac{2}{T_2}\tau + \ln\left(M_0\right) \tag{12}$$

Equation 12, on the other hand, calculates T_2 from the more-primitive Hahn spin-echo sequence, where the slope of the linear regression is again the negative reciprocal of the time constant T_2. However, since the Hahn spin-echo sequence only uses a single π-pulse, producing an echo a time τ equal to the time between the $\pi/2$-pulse and the π-pulse, the time t here is simply a fixed 2τ for each point. It is worth noting that due to the effects discussed on page 5, Hahn spin-echo plots often deviate significantly from

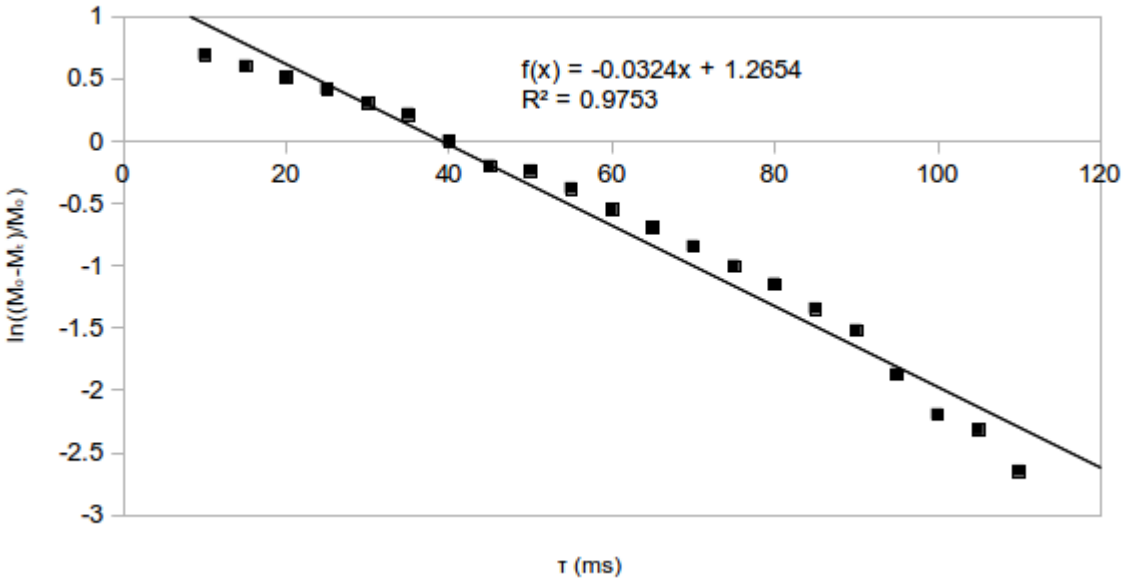

Figure 3: Inversion-recovery plot for mineral oil sample.

Sample	$\mathbf{T_1}$ (I-R) (ms)	$\mathbf{T_2}$ (M-G) (ms)	$\mathbf{T_2}$ (HS-E) (ms)
Mineral Oil	31(2)	78(2)	24(1)
$\mathbf{CuSO_4}$ (10 mM)	86(2)	111(7)	20.(3)
$\mathbf{CuSO_4}$ (50 mM)	16.3(4)	20.(1)	16(2)
$\mathbf{CuSO_4}$ (100 mM)	4.4(1)	9.6(4)	9.1(1)

Table 2: Collated results for T_2 and T_1 for all samples, using inversion-recovery, Meiboom-Gill, and Hahn spin-echo techniques.

expected linear trends.

Plots, with included regressions and equations, comprise Figures 3 to 14, and results are collated in Table 2 on page 9.

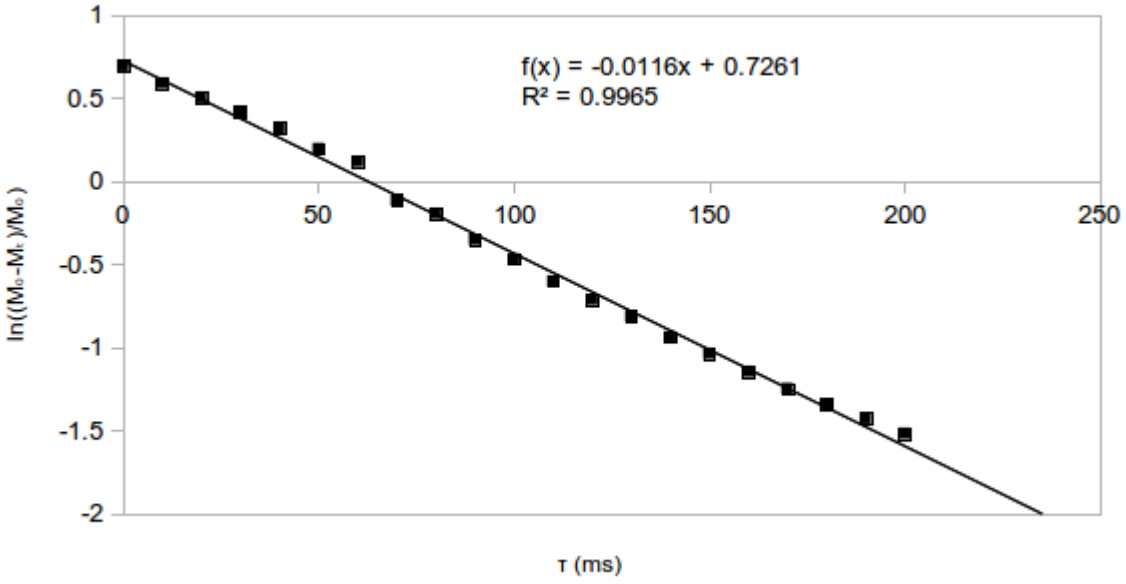

Figure 4: Inversion-recovery plot for 50 mM $CuSO_4$ sample.

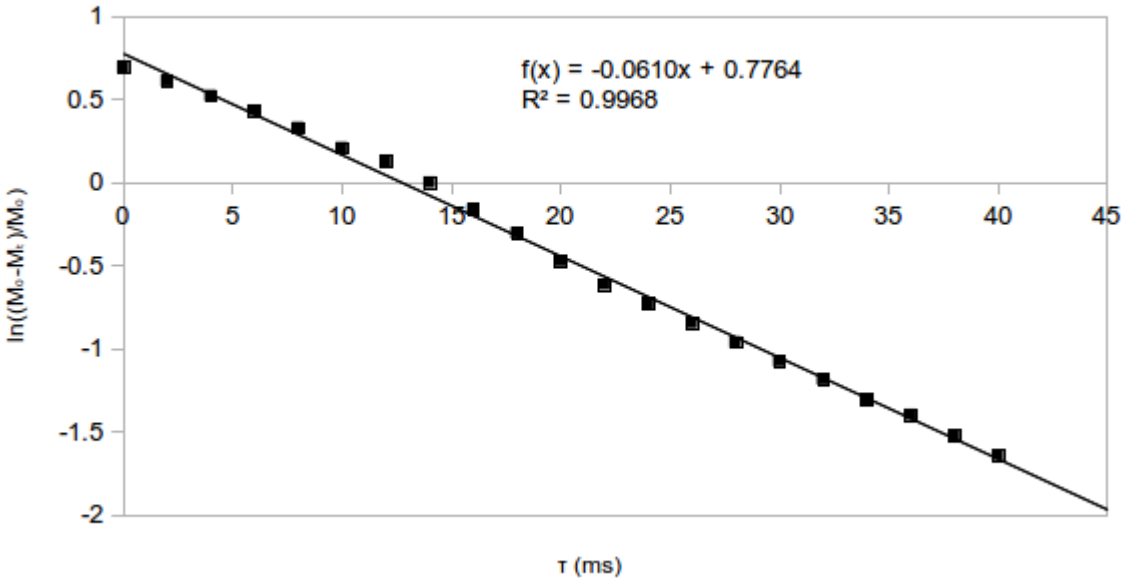

Figure 5: Inversion-recovery plot for 50 mM $CuSO_4$ sample.

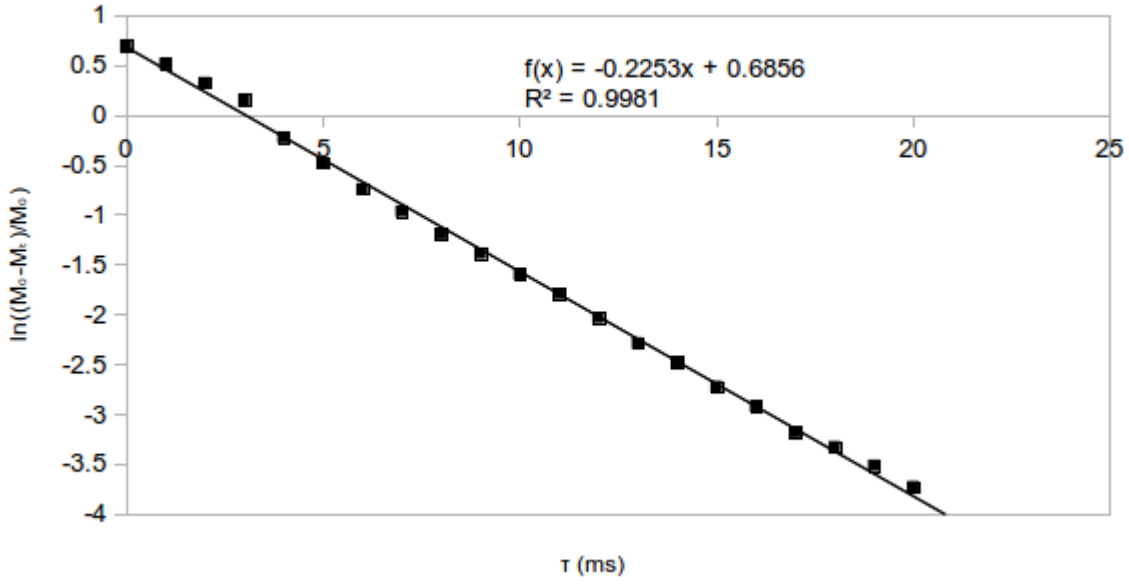

Figure 6: Inversion-recovery plot for 100 mM $CuSO_4$ sample.

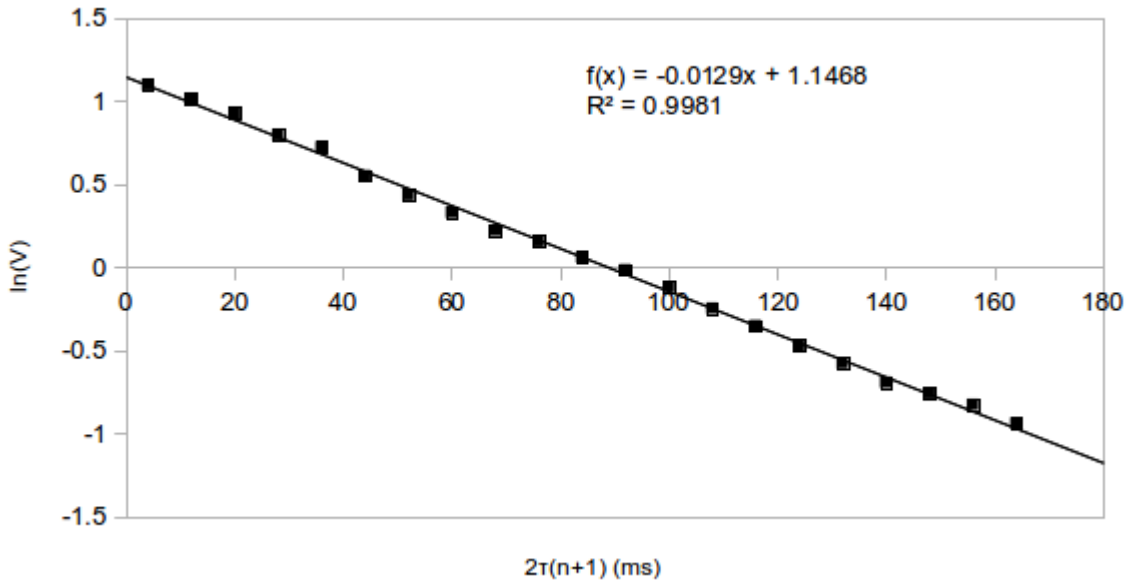

Figure 7: Meiboom-Gill plot for mineral oil sample.

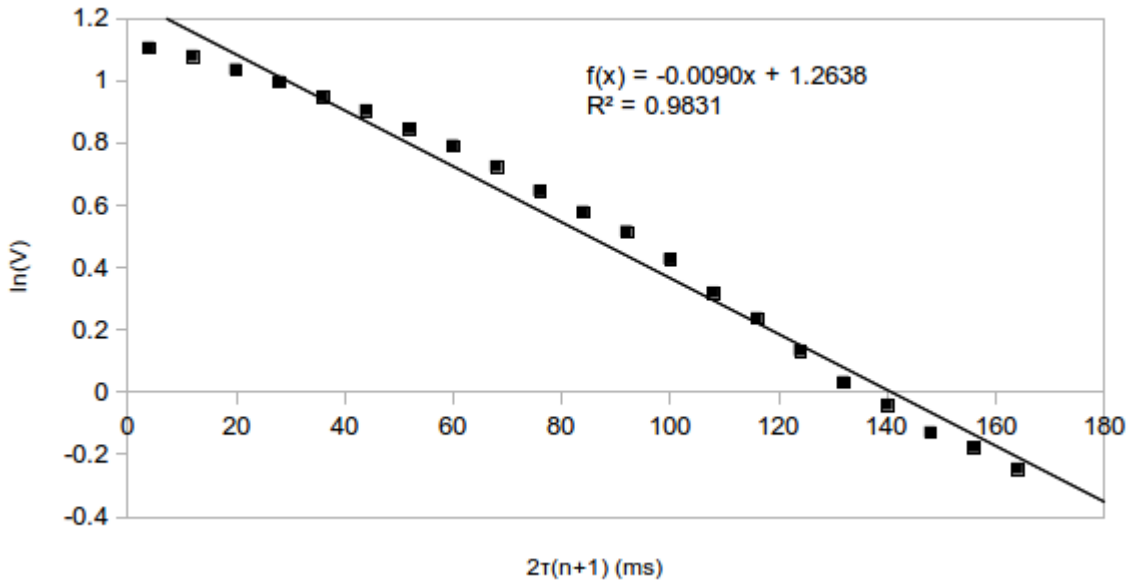

Figure 8: Meiboom-Gill plot for 10 mM $CuSO_4$ sample.

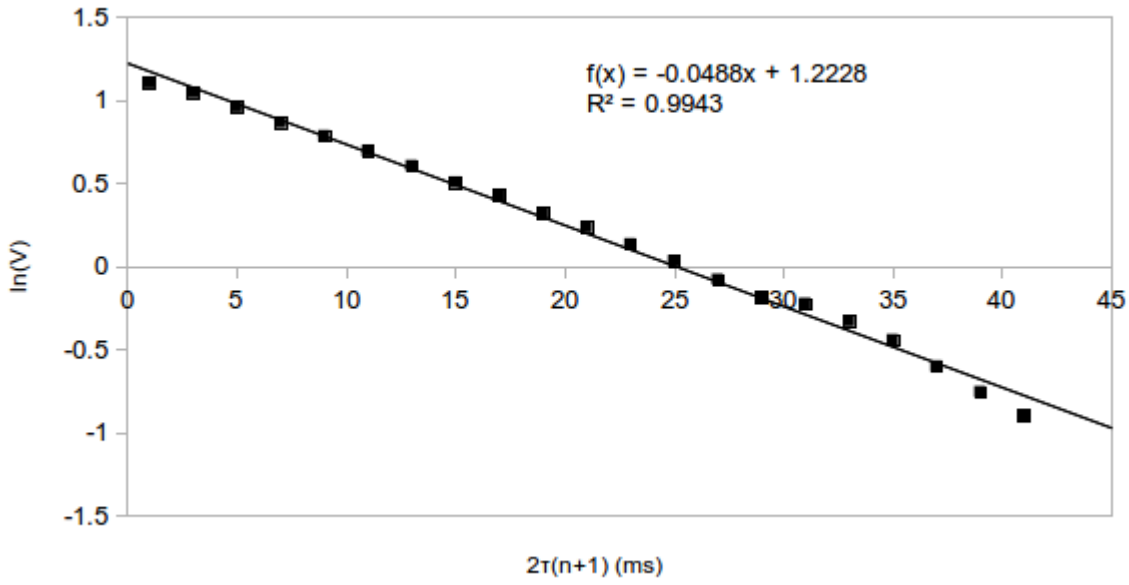

Figure 9: Meiboom-Gill plot for 50 mM $CuSO_4$ sample.

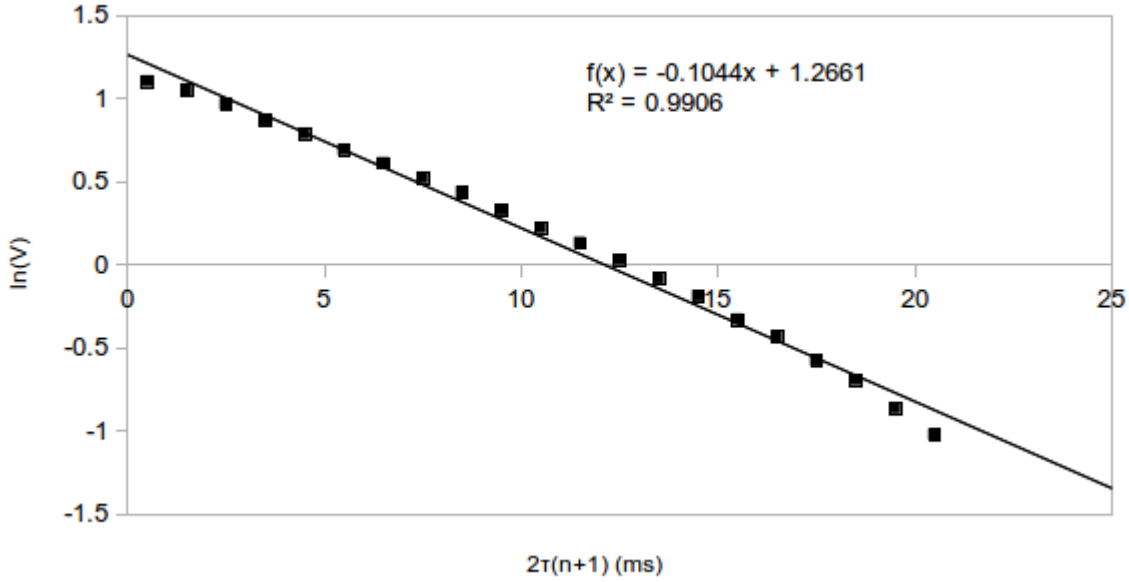

Figure 10: Meiboom-Gill plot for 100 mM $CuSO_4$ sample.

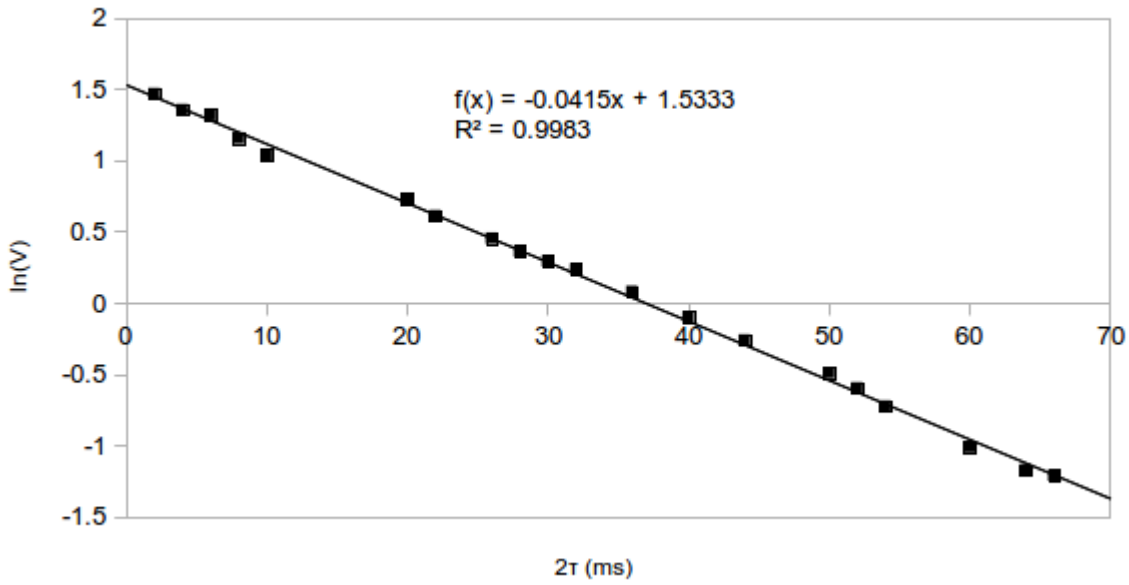

Figure 11: Hahn spin-echo plot for mineral oil sample.

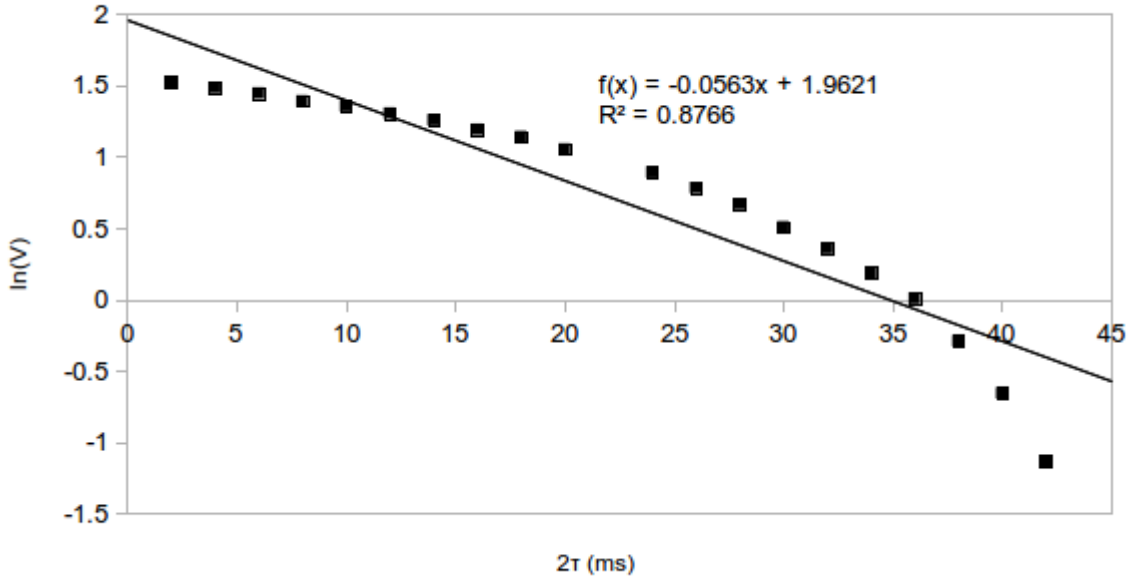

Figure 12: Hahn spin-echo plot for 10 mM $CuSO_4$ sample, showing deviations from linearity at larger delay times due to diffusion dependance.

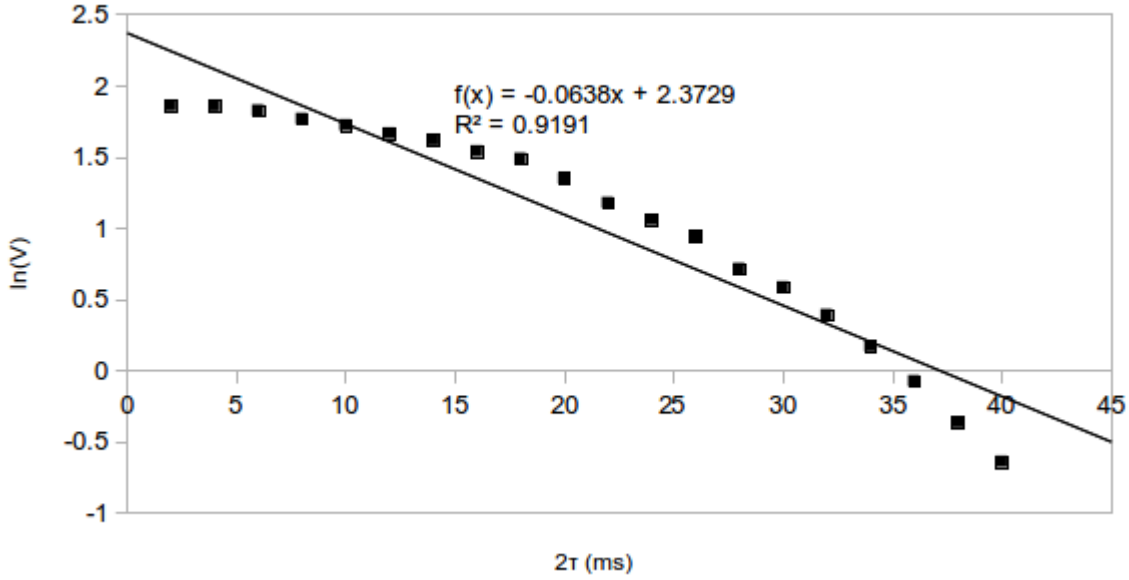

Figure 13: Hahn spin-echo plot for 50 mM $CuSO_4$ sample, showing deviations from linearity at larger delay times due to diffusion dependance.

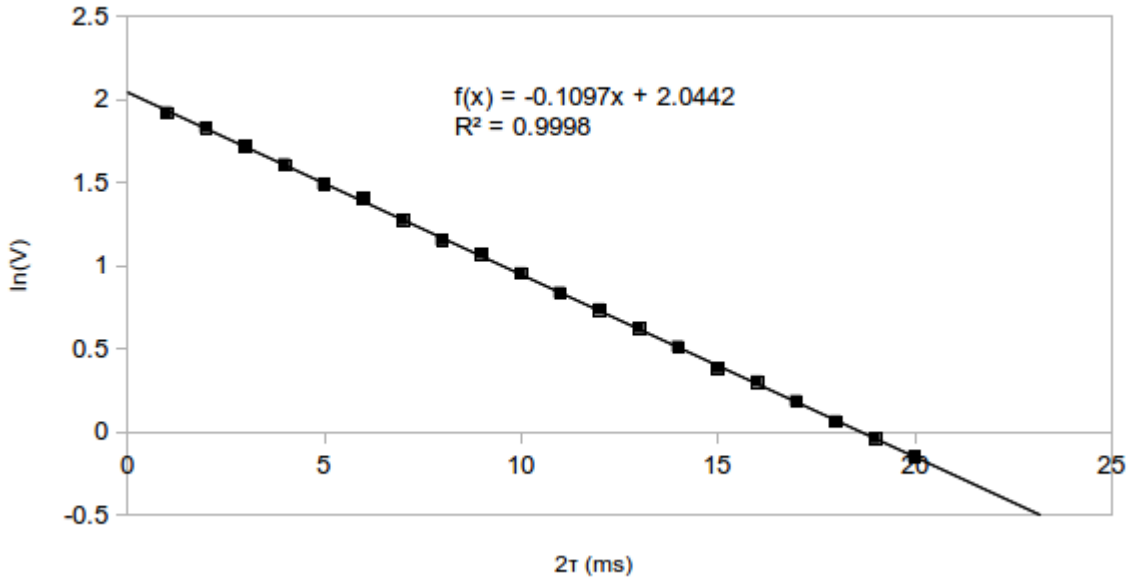

Figure 14: Hahn spin-echo plot for 100 mM $CuSO_4$ sample, showing no real deviations from linearity at larger delay times due to faster relaxation times.

4.2 Error Analysis

For each of the plots provided, linear regressions were created in Excel using the LINEST() function, which provided standard errors in the slope that were converted to standard deviations and subsequently 95% confidence intervals[4]. These intervals were then converted into relative errors and propagated into errors in T_1 and T_2 relaxation times, the negative reciprocals of the slope (seen in Table 2 on page 9).

Potential sources of error include the previously-mentioned inhomogeneity of the magnetic field, the effect of which is most noticeable at long relaxation times and at low viscosities. Variation in the placement of the sample tubes can increase the apparent inconsistency of the field in this regard. In theory, temperature fluctuations of the room across various samples would effect the relative population of states, but in practice this effect is likely to be negligible (as the splitting is very small anyway). Finally, improper degassing of the solutions could lead to the presence of dissolved O_2 gas, which is paramagnetic and can greatly affect the measured time constants[3].

5 Discussion

These results are reasonable, as they are of comparable order of magnitude to similar relaxation time constants reported in the literature[5]. The results collated in Table 2 on page 9 demonstrate the strong diffusion dependence of T_1 and T_2. In an idealized scenario, nuclei would experience a completely static applied magnetic field over the course of a pulse NMR experiment, either because they would remain perfectly still or the applied field would be completely unchanging with position. This position- and time-invariance allows for each measurement made over the course of the experiment to be directly comparable to each other. However, in practice, neither do nuclei remain perfectly stationary nor is the external magnetic field completely homogeneous. As a result, the detected magnetization is both position- and time-dependent, and the Brownian motion of particles in the sample introduces inherent uncertainties in the calculated relaxation times. Because the more viscous mineral oil results in slower Brownian motion of particles, it has a more linear regression, especially at longer time delays, than the 10 mM or 50 mM $CuSO_4$ samples.

However, as the concentration of copper increases, the defect of the Hahn spin-echo plots from a linear regression becomes less pronounced. This is because higher concentrations of copper (II) ions decrease the relaxation timescale; once the relaxation timescale becomes shorter than the diffusion timescale, each individual relaxation will more approximately take place in a homogenous external magnetic field. Copper (II) ions are capable of reducing the relaxation time because a solvated octahedral atom of d^9 Cu^{2+} is distorted by Jahn-Teller effects, and has an unpaired electron that renders each copper nucleus paramagnetic, allowing them to interact with hydrogen nuclei. Their magnetic fields, though small, are strong enough to locally increase the external magnetic field acting upon a hydrogen nucleus, reducing the T_1 relaxation time. They can also act to reduce the T_2 relaxation time by providing additional oscillating magnetic fields that can resonate at the Larmor precession frequency of protons, providing another way for spin-spin interactions to relax. Spin-spin interactions with copper (II) nuclei, however, are more powerful than comparable hydrogen interactions, so high concentrations of copper

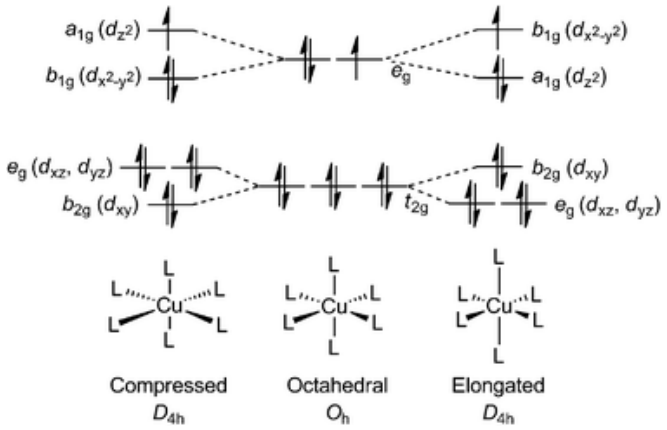

Figure 15: Jahn-Teller distortion of the d^9 Cu^{2+} ion complex produces a distorted octahedron with a net magnetic moment.

(II) ions will strongly discourage deviation from linearity at longer time delays[2]. (conversely, a solution of pure water with no copper (II) ions would suffer greatly as a result of the long relaxation time of water (on the order of seconds)[3] and the low viscosity of water. Between these two factors, a single particle is capable of diffusing a large distance in the time it takes for it to relax, causing large deviations from expected values).

These hypotheses are validated by our data, which shows that both T_1 and T_2 relaxation times decay exponentially with the concentration of copper (II) ions (Figures 16 and 17). For these purposes, we use exclusively Meiboom-Gill results for T_2, as (for reasons already explained) Hahn spin-echo sequences are not as accurate.

Additionally, our results showing the exponential decay of relaxation times with the concentration of paramagnetic ions are validated by the literature[5].

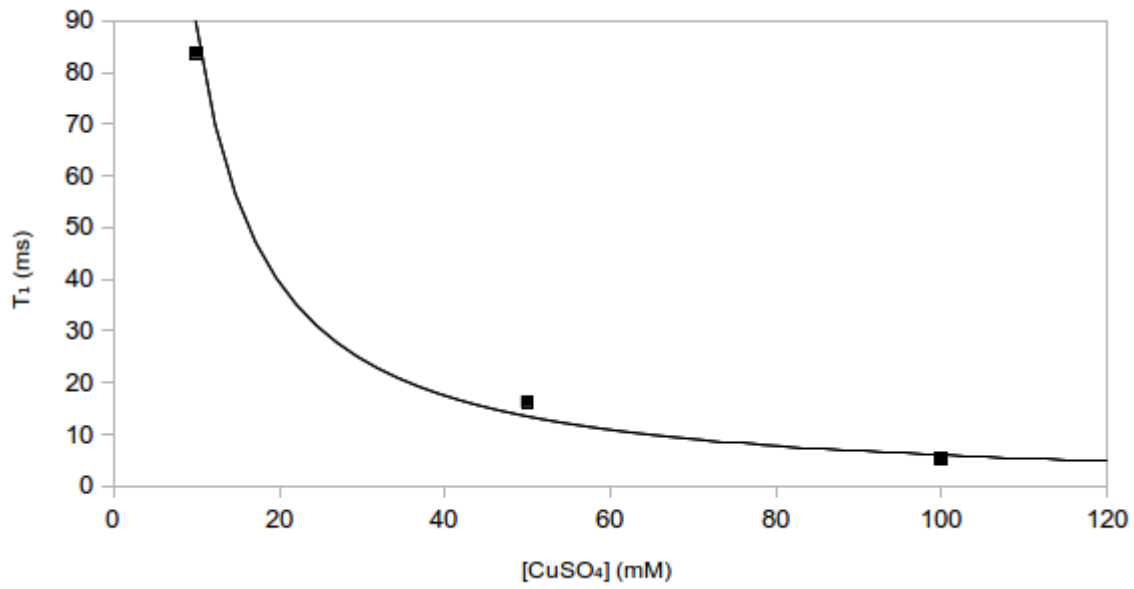

Figure 16: A plot of T_1 relaxation times by $CuSO_4$ concentration shows a decaying exponential relation.

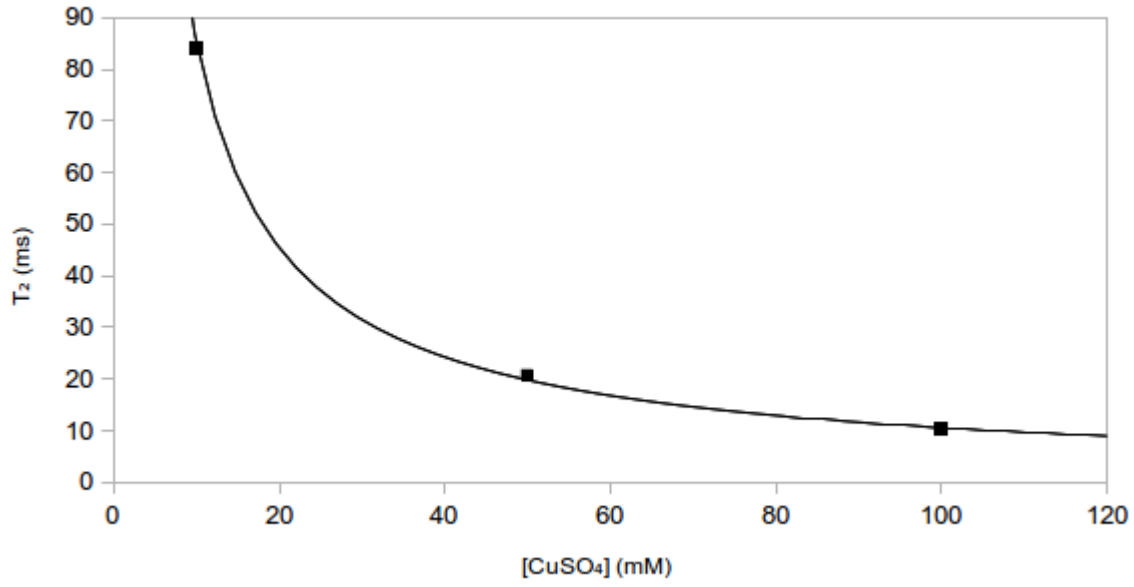

Figure 17: A plot of T_2 relaxation times by $CuSO_4$ concentration shows a decaying exponential relation.

6 Conclusion

In this experiment, pulsed nuclear magnetic resonance was used to calculate spin-lattice and spin-spin relaxation times for samples of varying viscosity as well as ionic strengths. T_1 relaxation times were calculated using an inversion-recovery sequence, whereas T_2 relaxation times were calculated using Meiboom-Gill spin-echo sequences. To demonstrate the diffusion dependence of relaxation times, T_2 relaxation times were also calculated with more primitive Hahn spin-echo sequences. Our data conclusively shows that relaxation times decrease exponentially with the concentration of paramagnetic Cu^{2+} ions, and that the more-viscous mineral oil displays a greater linear trend than dilute aqueous solutions at higher delay times, as a result of the Brownian motion of particles through inhomogeneous external magnetic fields.

7 Acknowledgments

The author would like to thank Jon Raberg, not just for his help elucidating a myriad of abstruse concepts in this lab report, but also for being an all-around outstanding GSI for the duration of the semester.

References

[1] http://www.pnas.org/content/71/4/1471.full.pdf&ei=NfSEVL6dMYjToAT18YGoAg&usg=AFQjC
ZG4PDjolBdF6WOFF3Kj887aig&sig2=YyvdQW28a6p1bQckQOk2oA

[2] Carr, H. Y. and Purcell, E.M., "Effects of diffusion on free precession in nuclear magnetic resonance experiments," Phys. Rev. 94(3):630-8. 1954.

[3] Friebolin, H. Basic One- and Two-Dimensional NMR Spectroscopy, 5th ed. Wiley VCH.

[4] Taylor, J. An Introduction to Error Analysis: The Study of Uncertainties in Physical Measurements, 2nd ed.; University Science Books: Sausalito, 1997.

[5] Bloembergen, N.; Purcell, E. M.; Pound, R. V. *Phys. Rev.* **1948**, 73, 679-712.

[6] Hahn, E. L. 1950. "Spin Echoes", *Phys. Rev.* 80 (4): 580-594.

[7] http://upload.wikimedia.org/wikipedia/commons/9/99/SpinEcho_GWM_stills.jpg

[8] Meiboom, S. and Gil, D., "Modified spin-echo method for measuring nuclear relaxation times." *Rev. Sci. Inst.* 29(8):688-691. 1958.

[9] Garland, C.W.; Nibler, J. W.; Shoemaker, D.P. *Experiments in Physical Chemistry*, 7th ed.; McGraw-Hill: New York, 2002

[10] Peng, P.; Caster, A.; Anderson, M.; Switz, N.; Brittman, S.; *Chemistry 125 Lab Manual*, Fall 2013 ed.; University of California, Berkeley: Berkeley, 2013.